Hindawi
Mathematical Problems in Engineering
Volume 2019, Article ID 2541707, 10 pages
https://doi.org/10.1155/2019/2541707

Research Article

Thermal Analysis of 2D FGM Beam Subjected to Thermal Loading Using Meshless Weighted Least-Square Method

H. M. Zhou, X. M. Zhang, and Z. Y. Wang

School of Mechanical and Power Engineering, Henan Polytechnic University, JiaoZuo, China

Correspondence should be addressed to H. M. Zhou; zhm_1979@163.com

Received 6 January 2019; Revised 18 March 2019; Accepted 10 April 2019; Published 30 April 2019

Academic Editor: Mohamed Shaat

The paper analyzed the thermal problem of the 2D FGM beam using meshless weighted least-square (MWLS) method. The MWLS as a meshless method is fully independent of mesh, and an approximate function was used to construct a series of linear equations to solve the unknown field variable, which avoided the troublesome task of numerical integration. The effectiveness and accuracy of the approach were illustrated by a clamped-clamped FGM beam which was subjected with interior heat source. The volume fraction of FGM beam was assumed to be given by a simple power law distribution. The effective material properties of the FGM beam were assumed to be temperature independent and calculated by Mori-Tanaka method. The results showed that a good agreement was achieved between the proposed meshless method and commercial COMSOL Multiphysics.

1. Introduction

FGMs can resist high temperatures and are proficient in reducing the thermal stress and have received more attention from the researchers [1]. Most of these researches on FGMs have been restricted to heat conduction analyses, thermal stress analyses, thermal buckling analyses, thermal vibration, and optimization problem. Various numerical techniques, such as the finite difference method (FDM) [2, 3], finite element method (FEM) [4–7], boundary element method (BEM) [8], or more recently developed meshless methods [9–23], have been developed for analyzing thermal related problems and other problems. Because of the complexity of the relevant governing equation, analytical solutions are usually difficult to obtain for those arbitrary geometry and complex boundary conditions, and the exact solutions are usually obtained based on classical plate theory, first-order shear deformation theory, high-order shear deformation theory, and so on [24, 25]. Compared with FEM, FDM, and BEM, the meshless methods are associated with a class of numerical techniques that approximate a given differential equation or a set of differential equations using global interpolations on the discrete nodes or background mesh, exhibiting the advantages of avoiding mesh generation, simple data preparation, easy postprocessing, and so forth.

Liu and Gu [15] introduced meshless methods and their programming, such as the element-free Galerkin (EFG) method [12, 16], the hp-clouds method, the meshless local Petrov-Galerkin (MLPG) method [9, 10], meshless Galerkin method using radial basis functions [11, 14, 21], the least-square method [20], and meshless point interpolation method [19]. The main advantage of the MLPG method compared with regular Galerkin-based methods is that no background mesh is used to evaluate various integrals appearing in the local weak formulation of problem, but it requires a high-order quadrature rule to obtain converged results and thus needs much more computational effort in terms of CPU time than that for the FEM. Ching and Chen [9] proposed the thermoelastic analysis of a functionally graded composite considering temperature-dependent thermomechanical properties by the MLPG method. Andrew and Senthil [12] proposed a methodology for the two-dimensional simulation and optimization of material distribution of functionally graded materials for thermomechanical processes using a genetic algorithm. Katsikadelis [13] employed the meshless analog equation method to solve the 2D elastostatic problem for inhomogeneous anisotropic. A meshless algorithm of fundamental solution coupling with radial basis functions based on analog equation theory was proposed to simulate the static thermal stress distribution in 2D FGMs [14].

Mierzwiczak et al. [17] presented the singular boundary method for steady-state nonlinear heat conduction problems. Bhavani et al. [26] solved thermoelastic equilibrium equations for a functionally graded beam to obtain the axial stress distribution. Sohn and Kim [27] analyzed static and dynamic stabilities of FG panels which are subjected to thermal and aerodynamic loads. Hiroyuki [28] presented a two-dimensional (2D) higher-order deformation theory presented for the evaluation of displacements and stresses in functionally graded (FG) plates subjected to thermal and mechanical loading.

Zhou et al. presented steady-state [29] and transient-state [30] heat conduction analysis of heterogeneous material using the meshless weighted least-square method. In this paper the pure meshless method (MWLS) was then extended to solve problems of thermoelastic analysis for the FGM beam with interior heat source. The volume fractions of constituent materials composing the FGM beam are assumed to be given by a simple power law distribution. Material properties of the FGM are obtained by Mori-Tanaka method. The paper is divided as follows: firstly, we give problem description and MWLS analysis about the thermal problem. Then, in order to demonstrate the efficiency and accuracy of the proposed method, numerical implementation is given in the next section. The last section includes some conclusions.

2. MWLS Analysis of the Thermal Problem

The solution of MWLS analysis to the thermal problem is described in this section. The shape functions in MWLS analysis is a moving least-squares approximation scheme which is originally developed for the smooth interpolation of irregularly distributed data.

2.1. The Moving Least-Square (MLS) Approximation Scheme. Construct the local approximate function $f^h(\boldsymbol{x})$ of an unknown field variable function $f(\boldsymbol{x})$ expressed as

$$f(x) \approx f^h(\boldsymbol{x}) = \boldsymbol{p}^T(\boldsymbol{x})\,\boldsymbol{a}(\boldsymbol{x}) \tag{1}$$

where $\boldsymbol{p}^T(\boldsymbol{x})$ is the basis function and the quadratic basis $\boldsymbol{p}^T(\boldsymbol{x}) = \{1, x, y, x^2, xy, y^2\}$ is used in this paper. In 2D space, the number of basis function m=6; $\boldsymbol{a}(\boldsymbol{x})$ are unknown coefficients, which are solved by minimizing a weighted discrete residual given as

$$\begin{aligned} JJ &= \sum_{I=1}^{N} \omega_I(\boldsymbol{x}) \left[f^h(\boldsymbol{x}, \boldsymbol{x}_I) - f(\boldsymbol{x}_I) \right]^2 \\ &= \sum_{I=1}^{N} \omega_I(\boldsymbol{x}) \left[\boldsymbol{p}^T(\boldsymbol{x})\,\boldsymbol{a}(\boldsymbol{x}) - f(\boldsymbol{x}_I) \right]^2 \end{aligned} \tag{2}$$

The minimum value of JJ may be achieved through differentiating with respect to $\boldsymbol{a}(\boldsymbol{x})$

$$\begin{aligned} \frac{\partial JJ}{\partial a_j(\boldsymbol{x})} &= 2\sum_{I=1}^{N} \omega_I(\boldsymbol{x}) \left[\sum_{i=1}^{m} p_i(\boldsymbol{x}_I)\, a_i(\boldsymbol{x}) - f_I \right] p_j(\boldsymbol{x}_I) \\ &= 0 \quad j = 1, 2, \ldots, m \end{aligned} \tag{3}$$

in which $\boldsymbol{x}_I$ are the positions of the N nodes, f_I refers to the nodal parameter of the field variable at node I, $f_I = f(\boldsymbol{x}_I)$. $\omega_I(\boldsymbol{x})$ is the weighting function and usually a compactly supported function that is only nonzero in a small neighborhood called the "support domain" of node $\boldsymbol{x}_I$. The exponential function is used in this study.

$$\omega(r) = \begin{cases} \dfrac{\left(\exp\left(-r^2\beta^2\right) - \exp\left(-\beta^2\right)\right)}{\left(1 - \exp\left(-\beta^2\right)\right)} & r \le 1 \\ 0 & r > 1 \end{cases} \tag{4}$$

where $r = \|\boldsymbol{x} - \boldsymbol{x}_I\|/d_{mI} = \sqrt{(x - x_I)^2 + (y - y_I)^2}/d_{mI}$ for circular support domain and β is a constant. d_{mI} denotes the radius of the circular support domain.

To obtain $\boldsymbol{a}(\boldsymbol{x})$, (3) can be rewritten in the matrix form

$$\boldsymbol{A}(\boldsymbol{x})\,\boldsymbol{a}(\boldsymbol{x}) = \boldsymbol{B}(\boldsymbol{x})\,\boldsymbol{f} \tag{5}$$

where $\boldsymbol{A}(\boldsymbol{x}) = \sum_{I=1}^{N} \omega_I(\boldsymbol{x})\boldsymbol{p}(\boldsymbol{x}_I)\boldsymbol{p}^T(\boldsymbol{x}_I)$, $\boldsymbol{B}(\boldsymbol{x}) = [\omega_1(\boldsymbol{x})p(\boldsymbol{x}_1)\ \ \omega_2(\boldsymbol{x})p(\boldsymbol{x}_2)\ \ \ldots\ \ \omega_N(\boldsymbol{x})p(\boldsymbol{x}_N)]$, $\boldsymbol{f} = [f(\boldsymbol{x}_1), f(\boldsymbol{x}_2), \ldots, f(\boldsymbol{x}_N)]^T$.

d_{mI} is chosen to make $\boldsymbol{A}(\boldsymbol{x})$ be the nonsingular matrix everywhere in the whole domain; however, the circular support domain must have enough neighborhood nodes. Through finding out the kkth nearest points of the evaluation point $\boldsymbol{x}$, the smallest support domain radius including these points can be obtained. The value of kk is gained by comparing some numerical examples with their analytical solutions in Zhou et al. [29, 30].

Solving $\boldsymbol{a}(\boldsymbol{x})$ from (5), coefficients $\boldsymbol{a}(\boldsymbol{x})$ can be obtained

$$\boldsymbol{a}(\boldsymbol{x}) = \boldsymbol{A}^{-1}(\boldsymbol{x})\,\boldsymbol{B}(\boldsymbol{x})\,\boldsymbol{f} \tag{6}$$

Substituting (6) back into (1) and removing unknown $\boldsymbol{a}(\boldsymbol{x})$, we have

$$f^h(\boldsymbol{x}) = \boldsymbol{p}^T(\boldsymbol{x})\,\boldsymbol{A}^{-1}(\boldsymbol{x})\,\boldsymbol{B}(\boldsymbol{x})\,\boldsymbol{f} = \boldsymbol{S}(\boldsymbol{x})\,\boldsymbol{f} \tag{7}$$

Set $\boldsymbol{p}^T(\boldsymbol{x})\boldsymbol{A}^{-1}(\boldsymbol{x})\boldsymbol{B}(\boldsymbol{x}) = \boldsymbol{S}(\boldsymbol{x})$, where $\boldsymbol{S}(\boldsymbol{x})$ is the shape function.

2.2. Heat Conduction Analysis of FGM Object. The steady-state heat conduction equation and the thermal boundary conditions of FGM objects are as follows, respectively,

$$k(\boldsymbol{x})\,\nabla^2 T(\boldsymbol{x}) + \nabla k(\boldsymbol{x}) \cdot \nabla T(\boldsymbol{x}) + Q = 0 \tag{8}$$

$$\begin{aligned} &\text{Dirichlet boundary: } T(\boldsymbol{x}) = \overline{T} \quad x \in \Gamma_1 \\ &\text{Neumann boundary: } \boldsymbol{n} \cdot k(\boldsymbol{x})\,\nabla T(\boldsymbol{x}) = \overline{q} \quad x \in \Gamma_2 \\ &\text{Mixed boundary: } \boldsymbol{n} \cdot k(\boldsymbol{x})\,\nabla T(\boldsymbol{x}) = h\left(T_\infty - T(\boldsymbol{x})\right) \\ &\qquad\qquad x \in \Gamma_3 \end{aligned} \tag{9}$$

where $T(\boldsymbol{x})$ is the temperature field on a fixed domain Ω surrounded by a closed boundary $\Gamma = \Gamma_1 + \Gamma_2 + \Gamma_3$. The variable $\boldsymbol{x}$ denotes the physical dimensions expressed in Cartesian coordinates, $\boldsymbol{x}$: (x, y). $\boldsymbol{n}$ is the outward surface normal. The

parameters k, T_∞, h and Q are the thermal conductivity, ambient temperature, the heat transfer coefficient, and the heat resource, respectively.

Substituting the unknown temperature field variable $T(\boldsymbol{x})$ of (8) with the approximate function of (7), the residuals are minimized in a least-squares manner,

$$\begin{aligned}\delta\prod &= \int_\Omega \delta f_J \left[k\nabla^2 S_J(x) + \nabla k \nabla S_J(x)\right] \\ &\cdot \left[k\nabla^2 S_I(x) f_I + \nabla k \nabla S_I(x) f_I + Q\right] d\Omega \\ &+ \int_{\Gamma_1} \delta f_J S_J(x) \left[S_I(x) f_I - \overline{f}\right] d\Gamma + \int_{\Gamma_2} \delta f_J \boldsymbol{n} \\ &\cdot k\nabla S_J(x) \cdot \left(\boldsymbol{n}\cdot k\nabla S_I(x) f_I - \overline{q}\right) d\Gamma \\ &+ \int_{\Gamma_3} \delta f_J \left(\boldsymbol{n}\cdot k\nabla S_J(x) + hS_J(x)\right) \\ &\cdot \left[\boldsymbol{n}\cdot k\nabla S_I(x) f_I - h\left(T_\infty - S_I(x) f_I\right)\right] d\Gamma\end{aligned} \tag{10}$$

We use an alternative discrete equation to avoid integration and (10) can be rewritten as

$$\begin{aligned}\delta\prod &= \delta f_J \sum_{s=1}^{N} \left[k_s\nabla^2 S_J(x_s) + \nabla k_s \nabla S_J(x_s)\right] \\ &\cdot \left[k_s\nabla^2 S_I(x_s) f_I + \nabla k_s \nabla S_I(x_s) f_I + Q\right] \\ &+ \delta f_J \sum_{s=1}^{N_1} S_J(x_s) \left[S_I(x_s) f_I - \overline{T}\right] \\ &+ \delta f_J \sum_{s=1}^{N_2} \boldsymbol{n}\cdot k_s\nabla S_J(x_s) \cdot \left(\boldsymbol{n}\cdot k_s\nabla S_I(x_s) f_I - \overline{q}\right) \\ &+ \delta f_J \sum_{s=1}^{N_3} \left[\boldsymbol{n}\cdot k_s\nabla S_J(x_s) + hS_J(x_s)\right] \\ &\cdot \left[\boldsymbol{n}\cdot k_s\nabla S_I(x) f_I - h\left(T_\infty - S_I(x_s) f_I\right)\right]\end{aligned} \tag{11}$$

The system equations of the MWLS method for solving steady-state heat conduction equations are written in a matrix form

$$KT = P \tag{12}$$

$$\begin{aligned}K &= \sum_{s=1}^{N} \left[k_s\nabla^2 S_J(x_s) + \nabla k_s \nabla S_J(x_s)\right] \\ &\cdot \left[k_s\nabla^2 S_I(x_s) + \nabla k_s \nabla S_I(x_s)\right] \\ &+ \sum_{s=1}^{N_1} S_J(x_s) S_I(x_s) + \sum_{s=1}^{N_2} \boldsymbol{n}\cdot k_s\nabla S_J(x_s)\boldsymbol{n} \\ &\cdot k_s\nabla S_I(x_s) + \sum_{s=1}^{N_3} \left[\boldsymbol{n}\cdot k_s\nabla S_J(x_s) + hS_J(x_s)\right] \\ &\cdot \left[\boldsymbol{n}\cdot k_s\nabla S_I(x) + hS_I(x)\right]\end{aligned} \tag{13}$$

$$\begin{aligned}P &= -\sum_{s=1}^{N} k_s\nabla^2 S_J(x_s) + \nabla k_s \nabla S_J(x_s)\,]Q \\ &+ \sum_{s=1}^{N_1} S_J(x_s)\overline{T} + \sum_{s=1}^{N_2} \boldsymbol{n}\cdot k_s\nabla S_J(x_s)\overline{q} \\ &+ \sum_{s=1}^{N_3} \left[\boldsymbol{n}\cdot k_s\nabla S_J(x_s) + hS_J(x_s)\right] hT_\infty\end{aligned} \tag{14}$$

where I and J refer to node indices, N_1, N_2, and N_3 is the number of interior nodes in the boundary Γ_1, Γ_2, and Γ_3, respectively.

2.3. Thermoelastic Analysis of FGM Object. Consider the 2D FGM anisotropic linear elastic body defined in the domain Ω bounded by Γ. The governing equation and boundary condition can be written in the following form disregarding the body forces

$$\sigma_{ij,j} = 0 \quad in\ \Omega \tag{15}$$

$$\begin{aligned}&\text{stress boundary condition: } \sigma_{ij}n_j - \overline{t}_i = 0 \quad \text{on } \Gamma_t \\ &\text{displacement boundary condition: } u_i = \overline{u}_i \quad \text{on } \Gamma_u\end{aligned} \tag{16}$$

in which σ_{ij} is the components of the Cauchy stress tensor. A comma followed by index j denotes the partial differentiation with respect to coordinate x_j of a material point. n_j is the unit outward normal to Γ. u_i are the displacement components, and $\overline{u}_i$ are the prescribed displacements on Γ_u. $\overline{t}_i$ are the prescribed traction on Γ_t. Γ_u and Γ_t are the complementary parts of the boundary Γ. MWLS analysis requires a discretization of the domain Ω; (15)-(16) becomes

$$\sigma_{ij,j}(\boldsymbol{x}_k) = 0 \quad \boldsymbol{x}_k \in \Omega,\ i,j = 1,2;\ k = 1,2,\ldots,N_\Omega \tag{17}$$

$$\sigma_{ij}(\boldsymbol{x}_k) n_j = \overline{t}_i(\boldsymbol{x}_k) \quad \boldsymbol{x}_k \in \Gamma_t,\ i,j = 1,2;\ k = 1,2,\ldots,N_t \tag{18}$$

$$u_i(\boldsymbol{x}_k) = \overline{u}_i(\boldsymbol{x}_k) \quad \boldsymbol{x}_k \in \Gamma_u,\ i = 1,2;\ k = 1,2,\ldots,N_u \tag{19}$$

where N_Ω, N_t, and N_u is the number of interior nodes in the domain Ω, in the boundary Γ_t and Γ_u, respectively.

Substituting σ_{ij}, u_i of (17)~(19) with the approximate function of (7),

$$\sum_{I=1}^{N} \boldsymbol{H}_I(x_k)\boldsymbol{f}_I = 0 \quad x_k \in \Omega,\ k = 1,2,\ldots,N_\Omega \tag{20}$$

$$\sum_{I=1}^{N} \boldsymbol{Q}_I(x_k)\boldsymbol{f}_I = \overline{\boldsymbol{t}}_k \quad x_k \in \Gamma_t,\ k = 1,2,\ldots,N_t \tag{21}$$

$$\sum_{I=1}^{N} \boldsymbol{N}_I(x_k)\boldsymbol{f}_I = \overline{\boldsymbol{u}}_k \quad x_k \in \Gamma_u,\ k = 1,2,\ldots,N_u \tag{22}$$

where $\boldsymbol{H}$, $\boldsymbol{Q}$, and $\boldsymbol{N}$ denote shape function similar to $\boldsymbol{S}$ of (7)

$$\boldsymbol{H}_I(x_k) = \frac{E}{1-\upsilon^2}\begin{bmatrix} \frac{\partial^2 N_I(x_k)}{\partial x^2} + \frac{1-\upsilon}{2}\frac{\partial^2 N_I(x_k)}{\partial y^2} & \frac{1+\upsilon}{2}\frac{\partial^2 N_I(x_k)}{\partial x \partial y} \\ \frac{1+\upsilon}{2}\frac{\partial^2 N_I(x_k)}{\partial x \partial y} & \frac{\partial^2 N_I(x_k)}{\partial y^2} + \frac{1-\upsilon}{2}\frac{\partial^2 N_I(x_k)}{\partial x^2} \end{bmatrix} \tag{23}$$

$$\boldsymbol{Q}_I(x_k) = \frac{E}{1-\upsilon^2}\begin{bmatrix} l\frac{\partial N_I(x_k)}{\partial x} + m\frac{1-\upsilon}{2}\frac{\partial N_I(x_k)}{\partial y} & l\upsilon\frac{\partial N_I(x_k)}{\partial y} + m\frac{1-\upsilon}{2}\frac{\partial N_I(x_k)}{\partial x} \\ m\upsilon\frac{\partial N_I(x_k)}{\partial x} + l\frac{1-\upsilon}{2}\frac{\partial N_I(x_k)}{\partial y} & m\frac{\partial N_I(x_k)}{\partial y} + l\frac{1-\upsilon}{2}\frac{\partial N_I(x_k)}{\partial x} \end{bmatrix} \tag{24}$$

$$\begin{aligned} \boldsymbol{N}_I &= \begin{bmatrix} \boldsymbol{N}_I(x_k) & 0 \\ 0 & \boldsymbol{N}_I(x_k) \end{bmatrix}, \\ \boldsymbol{f}_I &= \begin{bmatrix} f_{1I} \\ f_{2I} \end{bmatrix}, \\ \bar{\boldsymbol{t}}_k &= \begin{bmatrix} \bar{t}_1(x_k) \\ \bar{t}_2(x_k) \end{bmatrix}, \\ \bar{\boldsymbol{u}}_k &= \begin{bmatrix} \bar{u}_1(x_k) \\ \bar{u}_2(x_k) \end{bmatrix} \end{aligned} \tag{25}$$

where $l = \cos(No, x)$, $m = \cos(No, y)$; No is the normal vector of any point.

Substituting the unknown field variable σ_{ij} of (15)~(16) into (1), the residuals are minimized in a least-squares manner,

$$\begin{aligned} \Pi = &\int_\Omega \sigma_{ij,j}\sigma_{ik,k} d\Omega + \int_{\Gamma u} (u_i - \bar{u}_i)(u_i - \bar{u}_i)\, d\Gamma u \\ &+ \int_{\Gamma t} \left(\sigma_{ij} n_j - \bar{t}_i\right)\left(\sigma_{ij} n_j - \bar{t}_i\right) d\Gamma t \end{aligned} \tag{26}$$

Similar to (12) the system equations of the MWLS method for solving thermoelastic problem is written in the following matrix form

$$\boldsymbol{Kd} = \boldsymbol{P} \tag{27}$$

where

$$\begin{aligned} \boldsymbol{K} = &\sum_{s=1}^{N} \boldsymbol{H}^T(x_s)\boldsymbol{H}(x_s) + \sum_{s=1}^{N_u} \boldsymbol{N}^T(x_s)\boldsymbol{N}(x_s) \\ &+ \sum_{s=1}^{N_t} \boldsymbol{Q}^T(x_s)\boldsymbol{Q}(x_s) \end{aligned} \tag{28}$$

$$\boldsymbol{P} = \sum_{s=1}^{N_u} \boldsymbol{N}^T(x_s)\bar{u}_s + \sum_{s=1}^{N_t} \boldsymbol{Q}^T(x_s)\bar{t}_s \tag{29}$$

where $\boldsymbol{H}$, $\boldsymbol{Q}$, and $\boldsymbol{N}$ are obtained by (23)~(25) and $\boldsymbol{d}$ denotes the displacement of x, y, $[u_1, u_2]$.

The thermal stresses is written in the matrix form

$$\boldsymbol{\sigma} = \boldsymbol{D\varepsilon} - \boldsymbol{\beta}T \tag{30}$$

where $\boldsymbol{D}$ is the stiffness matrix for a linearly elastic, isotropic 2-D solid. ε is the infinitesimal strain vector.

$$\begin{aligned} \varepsilon &= \left[\frac{\partial u_1}{\partial x_1} \quad \frac{\partial u_2}{\partial x_2} \quad \frac{\partial u_2}{\partial x_1} + \frac{\partial u_1}{\partial x_2}\right]^T, \\ \boldsymbol{D} &= \frac{\overline{E}(x)}{1-\overline{\upsilon}(x)^2}\begin{bmatrix} 1 & \overline{\upsilon}(x) & 0 \\ \overline{\upsilon}(x) & 1 & 0 \\ 0 & 0 & \frac{(1-\overline{\upsilon}(x))}{2} \end{bmatrix} \end{aligned} \tag{31}$$

in which $\overline{E} = E$; $\overline{\upsilon} = \upsilon$; $\beta = (\alpha E/(1-\upsilon))\left\{\begin{smallmatrix}1\\1\\0\end{smallmatrix}\right\}$, for plane stress with E, υ and α denoting the Young's modulus, Poisson's ratio, and coefficient of thermal expansion, respectively, and $\overline{E} = E/(1-\upsilon^2)$; $\overline{\upsilon} = \upsilon/(1-\upsilon)$; $\beta = (\alpha E/(1-2\upsilon))\left\{\begin{smallmatrix}1\\1\\0\end{smallmatrix}\right\}$ for plane stain.

2.4. Material Properties. Two homogenization methods are often used to evaluate the effective material properties for FGMs. One is the rule of mixtures, and the other is the micromechanical model. The former is simply a linear rule of mixtures and the effective value can be determined by

$$P = P_1 V_1 + P_2 V_2 \tag{32}$$

where the volume fractions satisfy $V_1 + V_2 = 1$, and P may be elastic modulus E, bulk modulus G, Poisson's ratio ν, coefficient of thermal expansion a, thermal conductivity k, and shear modulus μ.

The most widely used micromechanical model is Mori-Tanaka model [9, 31]. It is the modified rule of mixtures and

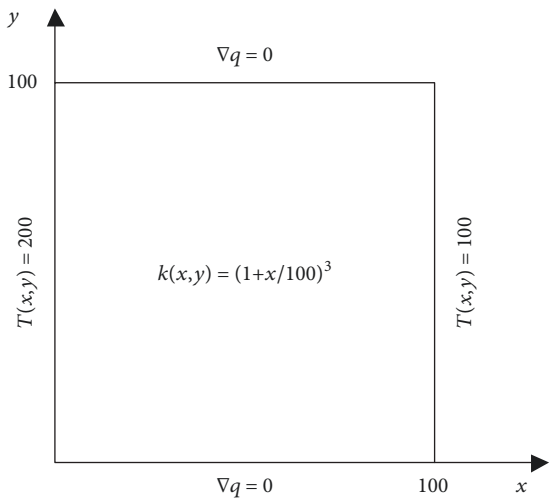

Figure 1: Geometry of square region and boundary conditions.

the effective material properties can be defined using the following relation,

$$k = k_1 + \frac{3k_1V_2(k_2 - k_1)}{3k_1 + V_1(k_2 - k_1)} \tag{33}$$

$$E = E_1 + \frac{V_2(3E_1 + 4\mu_1)(E_2 - E_1)}{3(1 - V_2)(E_2 - E_1) + 3E_1 + 4\mu_1} \tag{34}$$

$$\mu = \mu_1 + \frac{V_2(\mu_1 + ff_1)(\mu_2 - \mu_1)}{(1 - V_2)(\mu_2 - \mu_1) + \mu_1 + ff_1} \tag{35}$$

$$\alpha = \alpha_1 + \frac{E_2(E_1 - E)(\alpha_2 - \alpha_1)}{E(E_1 - E_2)} \tag{36}$$

where $G_1 = E_1/3(1-2\upsilon_1)$; $G_2 = E_2/3(1-2\upsilon_2)$; $\mu_1 = E_1/2(1+\upsilon_1)$; $\mu_2 = E_2/2(1+\upsilon_2)$; $ff_1 = \mu_1(9E_1 + 8\mu_1)/6(E_1 + 2\mu_1)$.

3. Numerical Results and Discussions

In order to demonstrate the efficiency and accuracy of the presented method, firstly, we choose a isotropic square region (Case 1) with defined boundary conditions; through heat conduction analysis the results are compared with the analytical solutions and FDM. Then a clamped-clamped FGM beam (Case 2) which was subjected with interior heat source is analyzed using MWLS method.

3.1. Case 1. A 100×100m isotropic square region is shown in Figure 1. The top and bottom boundaries are insulated. The left and right boundaries are assigned a temperature of 200°C and 100°C, respectively. The spatial variation of the thermal conductivity is taken to be cubic in the x-direction as $k(x, y) = (1 + x/100)^3$.

An analytical solution is given as

$$T(x, y) = \frac{800}{6}\left[\frac{1}{(1 + x/100)^2} + \frac{1}{2}\right] \tag{37}$$

Table 1: Maximum of relative error.

Cartesian grid	MWLS	FDM
10×10	0.15%	0.35%
20×20	0.05%	0.077%
30×30	0.024%	0.033%

Table 2: Material property.

Material property	Al	SiC
k(W/mK)	233	65
E(Pa)	7e10	4.27e11
υ	0.3	0.17
α (/K)	2.34e-5	4.3e-6

The design region is discretized as 20×20, $\beta = 4$ in (4), and the material properties are a linear rule of mixtures (Eq. (32)). The temperature field distribution is computed in Eq. (12)-(14) and shown in Figure 2. According to Wang et al. [32] the estimation rule is maximum of relative error% = $\max|(f - g)/f| \times 100\%$, in which f is the analytical solution and g is numerical solution. Then, our MWLS method is compared with FDM in different resolutions. The results are shown in Table 1. Obviously our method has a high precision compared with the analytical solution in spite of any resolution.

3.2. Case 2. A clamped-clamped FGM beam is shown in Figure 3, length L=1m, width D=0.5m, and thickness H=0.1m; material property is shown in Table 2, interior heat source Q=5e5W/m3; the spatial variation of the volume fraction of Al is taken to be a power law distribution in the y-direction as $V = (y/D)^a$.

The beam is assumed to be in a state of plane strain normal to the xy plane, and the design region is discretized as 31×15 and 61×30. The effective material properties are determined by the Mori-Tanaka model (Eq. (33)~(36)). In order to verify the proposed computational method, we do some comparisons between the MWLS and the commercial COMSOL Multiphysics for a homogeneous material (a=0), relevant results are shown in Figure 4 and listed in Table 3. The results obtained with the two methods are in good agreement in temperature field aspect; however, the x-displacements and y-displacement have a little difference in 31×15 grid and in 61×30 the results are in good agreement in Table 3. From Figure 4 we also can know that our method and COMSOL Multiphysics have the same distribution trend. The maximum temperature 361.3K is in the center (0.5, 0.25) of the beam.

For a=2, we analyzed the heat conduction and thermoelastic problem using MWLS method. Temperature field distribution, x-displacement, and y-displacement are plotted in Figures 5, 6, and 7, respectively. Figure 5 indicates that the maximum temperature 425.6K is higher than the homogeneous material of Figure 2(a), in the Cartesian coordinates (0.5, 0.179) of the beam. Figures 6 and 7 show that when subjected to temperature rise, the beam expands and the maximum y-displacement is located at the top middle of the beam. Then we do heat conduction analysis in different

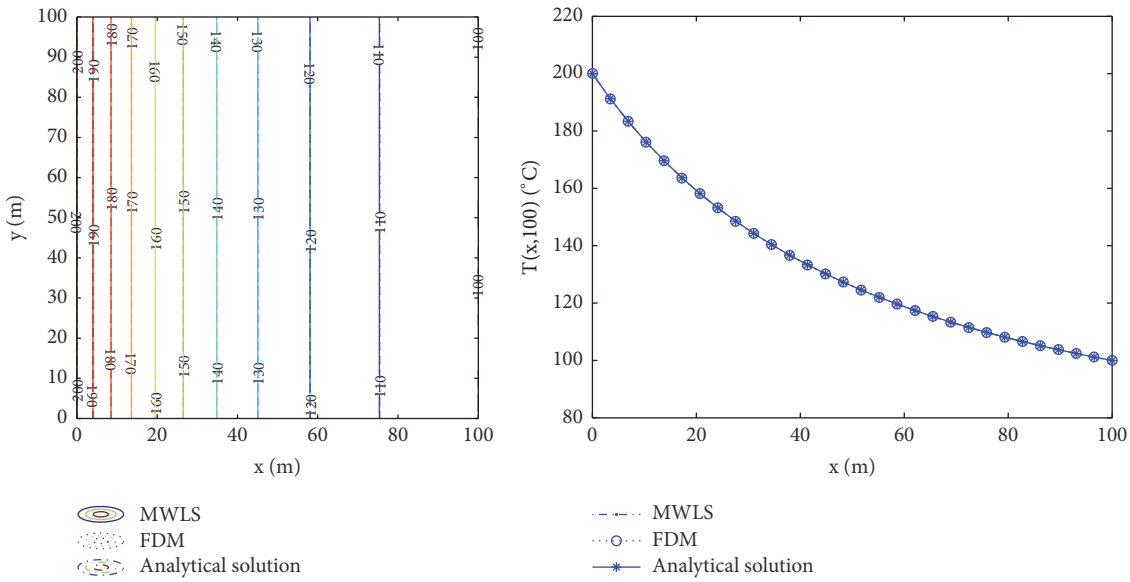

(a) 2D display (b) Top boundary

Figure 2: Temperature field distribution (20×20).

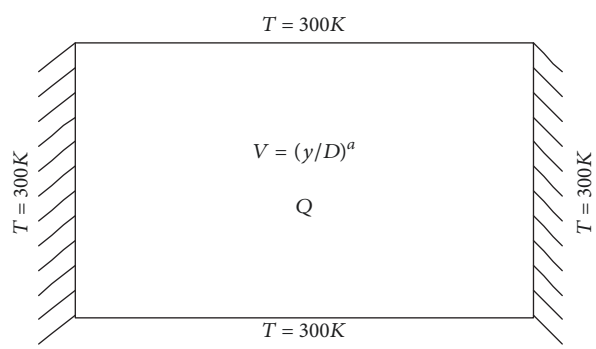

Figure 3: Initial condition.

material distribution in different heat source; the result is listed in Table 4. From Table 4, we can know that the maximum temperature of FGM model is higher than that of the fully metal model. Moreover, as the volume fraction index is increased, the maximum temperature increases. This is because for FGMs, when the volume fraction index is increased, the contained quantity of ceramic increases. Finally, to make a comparison, we do thermoelastic analysis and obtain thermal stresses in the neutral axis of the beam among a=0, a=2, and a=3, as shown in Figure 8. In Figures 8(a) and 8(c), the volume fraction of Al is gradually decreased from a=0 to a=3, the σx and σy stresses are in an upward trend. The maximum thermal stress always occurred in the vicinity of neutral axis of the beam from Figures 8(a), 8(c), and 8(d). The results also agreed well with the presented elasticity solutions of [26].

4. Conclusion

In this paper, a novel thermoelastic analysis of FGM beam based on MWLS method was presented. We do thermoelastic and heat conduction analysis aimed at a clamped-clamped thick beam which is subjected with interior heat source. The FGM beam is assumed to be given by a simple power law distribution. Material properties of the FGM beam are obtained by Mori-Tanaka method. Through being compared with analytical solution and the commercial software of COMSOL Multiphysics, the effectiveness and accuracy are verified. We also listed the comparison of thermal stresses with the variation of power law index. The present method of analysis will be also useful in the design and optimization of FGM objects.

Nomenclature

$\boldsymbol{a}(\boldsymbol{x})$:	Coefficient
$\boldsymbol{A}(\boldsymbol{x}), \boldsymbol{B}(\boldsymbol{x})$:	Matrices of computation
d_{mI}:	Radius of the circular support domain
f_I:	The nodal parameter of the field variable at node I
I, J:	Node indices
k:	Thermal conductivity

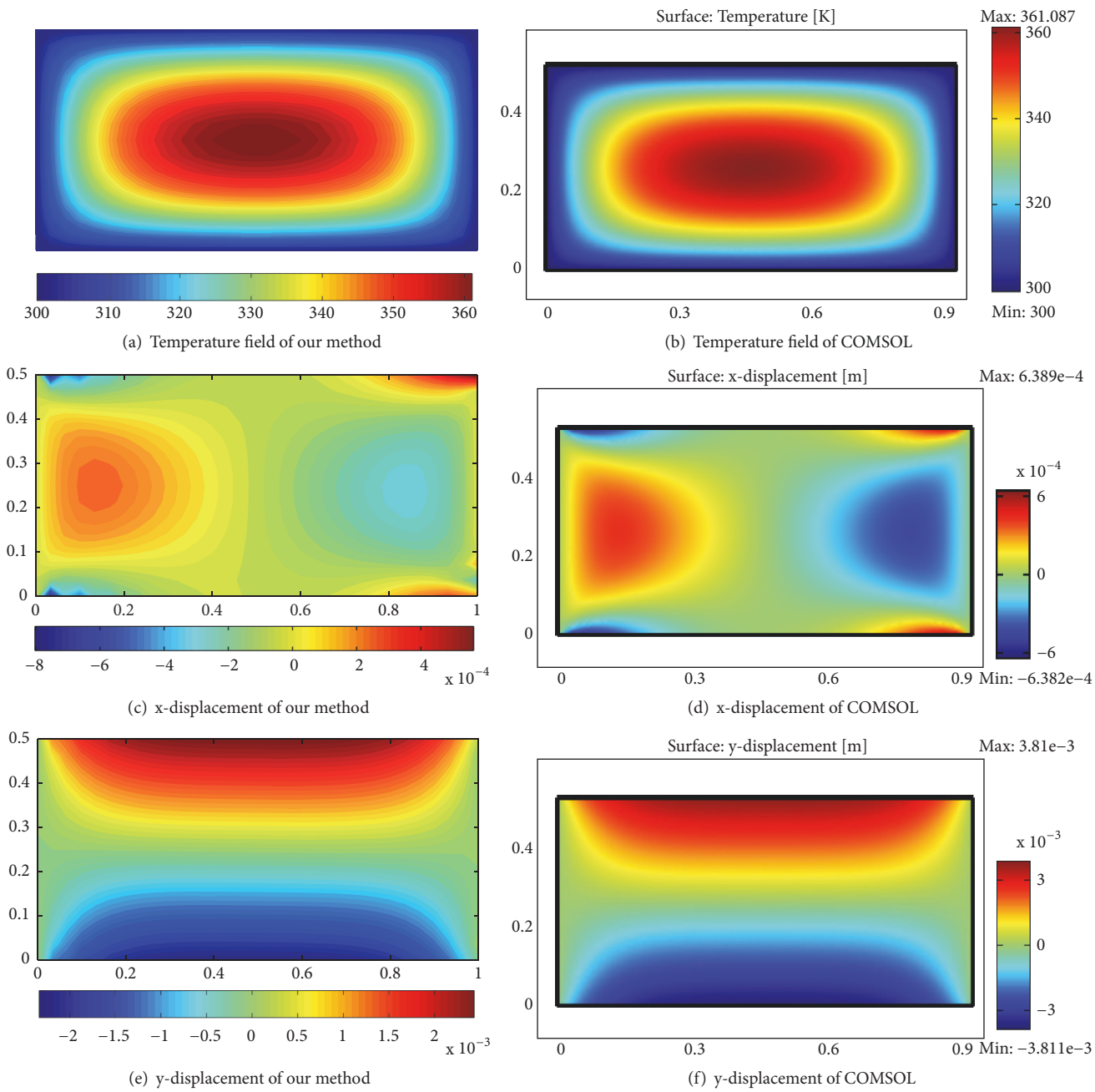

(a) Temperature field of our method

(b) Temperature field of COMSOL

(c) x-displacement of our method

(d) x-displacement of COMSOL

(e) y-displacement of our method

(f) y-displacement of COMSOL

Figure 4: Comparison of our method with COMOSOL of a=0.

Table 3: Comparison of MWLS method and COMSOL Multiphysics.

method	Temperature/K		X displacement /mm		Y displacement/mm	
	maximum	minimum	maximum	minimum	maximum	minimum
MWLS (31×15)	361.8	300	.596	-.873	2.95	-2.8
MWLS (61×30)	361.3	300	.71	-.72	3.88	-3.84
COMSOL (948 triangle mesh)	361.1	300	.639	-.639	3.81	-3.81

Table 4: Comparison of different material distribution in different heat source.

MWLS (31×15)	Temperature/K Q=5e5W/m^3		Temperature/K Q=5e6W/m^3	
	maximum	minimum	maximum	minimum
a=0	361.8	300	910.8	300
a=2	425.6	300	1558.2	300
a=3	436.1	300	1660.9	300

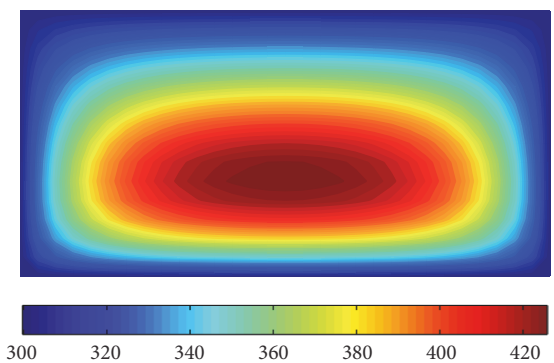

Figure 5: Distribution of temperature field.

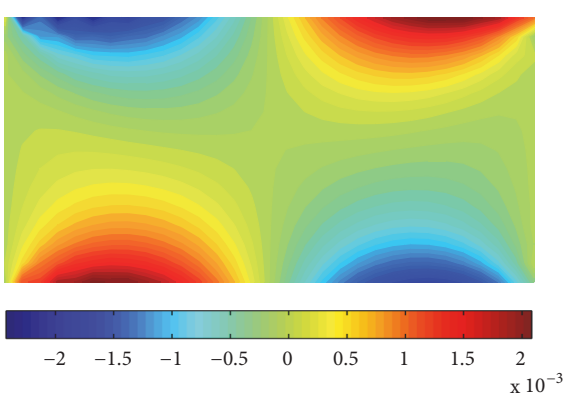

Figure 6: x-displacement/m.

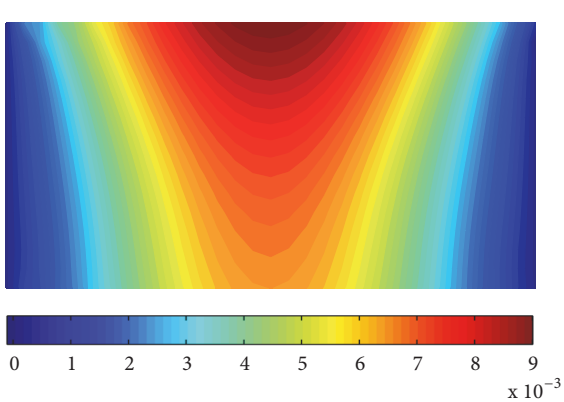

Figure 7: y-displacement/m.

kk:	Number of neighbor points
N:	Number of nodes
$\boldsymbol{n}$:	Outward surface normal
$\boldsymbol{S}(\boldsymbol{x}), \boldsymbol{N}(\boldsymbol{x}), \boldsymbol{H}(x), \boldsymbol{Q}(x)$:	Shape functions
$N1, N2, N3$:	Number of interior nodes in the boundary Γ_1, Γ_2 and Γ_3
$\boldsymbol{p}(\boldsymbol{x})$:	Basis function
Q:	Heat source
σ_{ij}:	Components of the Cauchy stress tensor
Γ_u, Γ_t:	Complementary parts of the boundary Γ
D:	Stiffness matrix
E:	Young's modulus
α:	Coefficient of thermal expansion
V:	Volume fraction
T:	Temperature
T_∞:	Ambient temperature
h:	The heat transfer coefficient
$f^h(\boldsymbol{x})$:	The moving least-square approximation function
$\boldsymbol{x}_I$:	The positions of the nodes
Ω:	Fixed domain
Γ:	Closed boundary of Ω
Γ_1:	Dirichlet boundary
Γ_2:	Neumann boundary
Γ_3:	Mixed boundary
$\omega_I(\boldsymbol{x})$:	Weight functions
q:	Normal heat flux
$\bar{t}_i$:	Given traction on Γ_t
u_i:	Displacement components
d:	Displacement of x, y
ε:	Infinitesimal strain vector
υ:	Poisson's ratio
μ:	Shear modulus
G:	Bulk modulus.

Data Availability

The data used to support the findings of this study are included within the article.

Conflicts of Interest

The authors declare that they have no conflicts of interest.

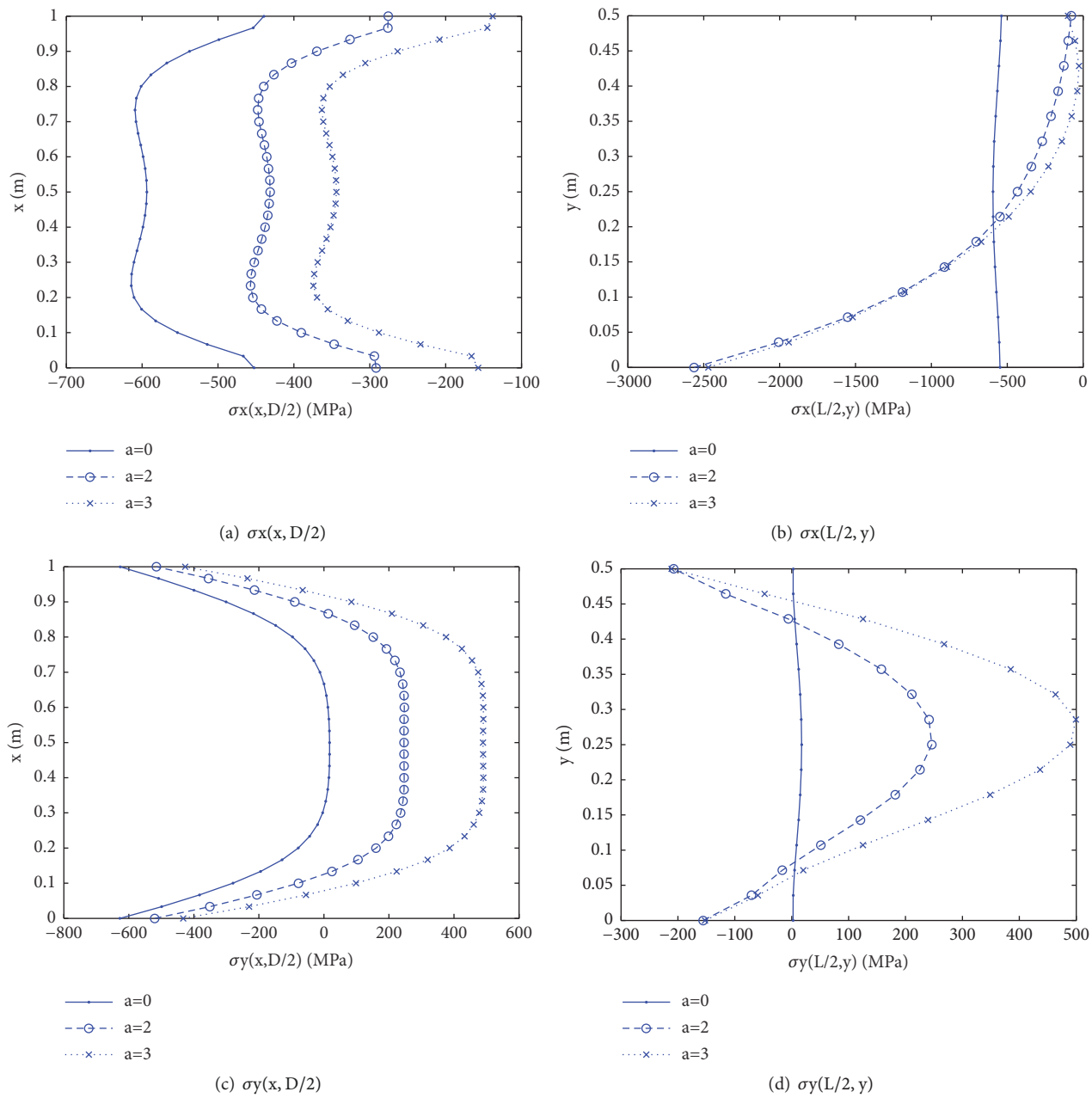

Figure 8: Stress results comparison of thermoelastic analysis among a=0, a=2, and a=3.

Acknowledgments

The work described in this paper was supported by a grant from the National Natural Science Foundation of China (Projects No. 51505131, U1504106) and Program for Innovative Research Team (No. T2017-3) of Henan Polytechnic University. The correlative members of the projects are hereby acknowledged.

References

[1] K. Swaminathan and D. Sangeetha, "Thermal analysis of FGM plates – A critical review of various modeling techniques and solution methods," *Composite Structures*, vol. 160, pp. 43–60, 2017.

[2] S. Turteltaub, "Optimal control and optimization of functionally graded materials for thermomechanical processes," *International Journal of Solids and Structures*, vol. 39, no. 12, pp. 3175–3197, 2002.

[3] J. R. Cho and D. Y. Ha, "Volume fraction optimization for minimizing thermal stress in Ni-Al2O3 functionally graded materials," *Materials Science and Engineering: A Structural Materials: Properties, Microstructure and Processing*, vol. 334, no. 1-2, pp. 147–155, 2002.

[4] K.-S. Na and J.-H. Kim, "Thermal postbuckling investigations of functionally graded plates using 3-D finite element method,"

Finite Elements in Analysis and Design, vol. 42, no. 8-9, pp. 749–756, 2006.

[5] X. Y. Kou and S. T. Tan, "A systematic approach for integrated computer-aided design and finite element analysis of functionally-graded-material objects," *Materials and Corrosion*, vol. 28, no. 10, pp. 2549–2565, 2007.

[6] M. Lezgy-Nazargah, "Fully coupled thermo-mechanical analysis of bi-directional FGM beams using NURBS isogeometric finite element approach," *Aerospace Science and Technology*, vol. 45, pp. 154–164, 2015.

[7] A. Najibi and R. Talebitooti, "Nonlinear transient thermoelastic analysis of a 2D-FGM thick hollow finite length cylinder," *Composites Part B: Engineering*, vol. 111, pp. 211–227, 2017.

[8] A. Sutradhar and G. H. Paulino, "The simple boundary element method for transient heat conduction in functionally graded materials," *Computer Methods Applied Mechanics and Engineering*, vol. 193, no. 42-44, pp. 4511–4539, 2004.

[9] H. K. Ching and J. K. Chen, "Thermal stress analysis of functionally graded composites with temperature-dependent material properties," *Journal of Mechanics of Materials and Structures*, vol. 2, no. 4, pp. 633–654, 2007.

[10] H. K. Ching and S. C. Yen, "Meshless local Petrov-Galerkin analysis for 2D functionally graded elastic solids under mechanical and thermal loads," *Composites Part B: Engineering*, vol. 36, no. 3, pp. 223–240, 2005.

[11] H. Wang and Q.-H. Qin, "Meshless approach for thermo-mechanical analysis of functionally graded materials," *Engineering Analysis with Boundary Elements*, vol. 32, no. 9, pp. 704–712, 2008.

[12] A. J. Goupee and S. S. Vel, "Two-dimensional optimization of material composition of functionally graded materials using meshless analyses and a genetic algorithm," *Computer Methods Applied Mechanics and Engineering*, vol. 195, no. 44-47, pp. 5926–5948, 2006.

[13] J. T. Katsikadelis, "The 2D elastostatic problem in inhomogeneous anisotropic bodies by the meshless analog equation method (MAEM)," *Engineering Analysis with Boundary Elements*, vol. 32, no. 12, pp. 997–1005, 2008.

[14] D. F. Gilhooley, J. R. Xiao, R. C. Batra, M. A. McCarthy, and J. W. Gillespie Jr., "Two-dimensional stress analysis of functionally graded solids using the MLPG method with radial basis functions," *Computational Materials Science*, vol. 41, no. 4, pp. 467–481, 2008.

[15] G. Liu and Y. T. RGu, *An Introduction to Meshfree Methods And Their Programming*, Springer, Berlin, Germany, 2005.

[16] S. Senthil, V. J. Goupee, and A. J. Goupee, "A methodology for the optimization of material composition of functionally graded materials," in *Proceedings of the NSF DMII Grantees' Conference*, Scottsdale, Ariz, USA, 2005.

[17] M. Mierzwiczak, W. Chen, and Z.-J. Fu, "The singular boundary method for steady-state nonlinear heat conduction problem with temperature-dependent thermal conductivity," *International Journal of Heat and Mass Transfer*, vol. 91, pp. 205–217, 2015.

[18] Z.-J. Fu, W. Chen, and Q.-H. Qin, "Boundary knot method for heat conduction in nonlinear functionally graded material," *Engineering Analysis with Boundary Elements*, vol. 35, no. 5, pp. 729–734, 2011.

[19] V. N. Van Do and C.-H. Lee, "Nonlinear analyses of FGM plates in bending by using a modified radial point interpolation meshfree method," *Applied Mathematical Modelling: Simulation and Computation for Engineering and Environmental Systems*, vol. 57, pp. 1–20, 2018.

[20] L. Sator, V. Sladek, and J. Sladek, "Bending of FGM plates under thermal load: classical thermoelasticity analysis by a meshless method," *Composites Part B: Engineering*, vol. 146, pp. 176–188, 2018.

[21] J. Lin, S. Y. Reutskiy, and J. Lu, "A novel meshless method for fully nonlinear advection-diffusion-reaction problems to model transfer in anisotropic media," *Applied Mathematics and Computation*, vol. 339, pp. 459–476, 2018.

[22] J. Lin, C. Zhang, L. Sun, and J. Lu, "Simulation of seismic wave scattering by embedded cavities in an elastic half-plane using the novel singular boundary method," *Advances in Applied Mathematics and Mechanics*, vol. 10, no. 2, pp. 322–342, 2018.

[23] J. Lin, C. S. Chen, C.-S. Liu, and J. Lu, "Fast simulation of multi-dimensional wave problems by the sparse scheme of the method of fundamental solutions," *Computers & Mathematics with Applications*, vol. 72, no. 3, pp. 555–567, 2016.

[24] S. S. Vel and R. C. Batra, "Exact solution for thermoelastic deformations of functionally graded thick rectangular plates," *AIAA Journal*, vol. 40, no. 7, pp. 1421–1433, 2002.

[25] A. Alibeigloo, "Exact solution for thermo-elastic response of functionally graded rectangular plates," *Composite Structures*, vol. 92, no. 1, pp. 113–121, 2010.

[26] B. V. Sankar and J. T. Tzeng, "Thermal stresses in functionally graded beams," *AIAA Journal*, vol. 40, no. 6, pp. 1228–1232, 2002.

[27] K.-J. Sohn and J.-H. Kim, "Structural stability of functionally graded panels subjected to aero-thermal loads," *Composite Structures*, vol. 82, no. 3, pp. 317–325, 2008.

[28] H. Matsunaga, "Stress analysis of functionally graded plates subjected to thermal and mechanical loadings," *Composite Structures*, vol. 87, no. 4, pp. 344–357, 2009.

[29] H. Zhou, Z. Liu, and B. Lu, "Heat conduction analysis of heterogeneous objects based on multi-color distance field," *Materials & Design*, vol. 31, no. 7, pp. 3331–3338, 2010.

[30] H. M. Zhou, W. H. Zhou, G. Qin, Z. Y. Wang, and P. M. Ming, "Transient heat conduction analysis for distance-field-based irregular geometries using the meshless weighted least-square method," *Numerical Heat Transfer, Part B: Fundamentals*, vol. 71, no. 5, pp. 456–466, 2017.

[31] X. Peng, N. Hu, H. Zheng, and H. Fukunaga, "Evaluation of mechanical properties of particulate composites with a combined self-consistent and Mori-Tanaka approach," *Mechanics of Materials*, vol. 41, no. 12, pp. 1288–1297, 2009.

[32] H. Wang, Q. H. Qin, and Y. L. Kang, "A new meshless method for steady-state heat conduction problems in anisotropic and inhomogeneous media," *Archive of Applied Mechanics*, vol. 74, no. 8, pp. 563–579, 2005.